Exp Brain Res (2014) 232:2391–2405
DOI 10.1007/s00221-014-3936-7

RESEARCH ARTICLE

Cell directional spread determines accuracy, precision, and length of the neuronal population vector

Apostolos P. Georgopoulos

Received: 6 December 2013 / Accepted: 24 March 2014 / Published online: 12 April 2014

Abstract The neuronal population vector (NPV) for movement direction is the sum of weighted neuronal directional contributions. Based on theoretical considerations, we proposed recently that the sharpness of tuning will impact the directional precision, accuracy, and length of the NPV, such that sharper tuning will yield NPV with higher precision, higher accuracy, and shorter length (Mahan and Georgopoulos in Front Neural Circuits 7:92, 2013). Furthermore, we proposed that controlling the inhibitory drive in a local network could be the mechanism by which the sharpness of directional tuning would be varied, resulting in a continuous specification and control of movement's directional precision, accuracy, and speed (Mahan and Georgopoulos in Front Neural Circuits 7:92, 2013, Fig. 5). As a first step in testing this idea, here we analyzed data from 899 cells recorded in the motor cortex during performance of a center → out task. There were two major findings. First, directional selectivity varied with cell activity, such that it was higher in cells with lower mean discharge rates. And second, NPVs calculated from subsets of cells with higher directional selectivity (and, correspondingly, lower mean discharge rates) were more accurate (i.e., closer to the movement), precise (i.e., less variable), and shorter (i.e., slower; Schwartz in Science 265:540–542, 1994). These findings confirm our predictions above made from modeling (Mahan and Georgopoulos in Front Neural Circuits 7:92, 2013) and provide a simple mechanism by which desired attributes of the directional motor command can be implemented. We hypothesize that the inhibitory drive in a local network is controlled directly and independently of recurrent collaterals or common excitatory inputs to other cells. This could be achieved by a private excitation/inhibition of key inhibitory interneurons in a way similar to that in operation for Renshaw cells in the spinal cord. The presence of such a private line of inhibitory control remains to be investigated.

Keywords Directional tuning · Neuronal population vector · Cortical inhibition

A. P. Georgopoulos (✉)
Department of Veterans Affairs, Brain Sciences Center (11B), Minneapolis Health Care System, One Veterans Drive, Minneapolis, MN 55417, USA
e-mail: omega@umn.edu

A. P. Georgopoulos
Department of Neuroscience, University of Minnesota Medical School, Minneapolis, MN 55455, USA

Introduction

Directional tuning is ubiquitous in the brain (Mahan and Georgopoulos 2013) and is present for 2-D (Georgopoulos et al. 1982) and 3-D arm movements (Schwartz et al. 1988). In 1983, the neuronal population vector (NPV) code was proposed for 2-D movements (Georgopoulos et al. 1983), a code that worked well for 3-D movements (Georgopoulos et al. 1986, 1988). The NPV is the vector sum of weighted directional contributions of individual cells in a population. Specifically, the preferred directions of cells are weighted by a measure related to cell activity (see Appendix in Georgopoulos et al. 1988): The weight can be the raw discharge rate, the raw discharge rate adjusted with respect to the average firing rate, or the predicted discharge rate estimated from the tuning function. In all the published studies, the NPV has been calculated from ensembles of directionally tuned cells, irrespective of their tuning characteristics. In a recent paper (Mahan and Georgopoulos 2013), we showed

by modeling that the sharpness of directional tuning can impact the directional accuracy of the NPV. Here, we confirm this prediction directly by the results of analysis of neurophysiological recordings from the motor cortex of monkeys performing a center-out task.

Materials and methods

Neurophysiological data

Previously recorded data (from 1980 to 1987) were used for these analyses. Eight monkeys performed the 2-D center-out task described in detail in Georgopoulos et al. (1982). Valid data from 899 cells recorded in the motor cortex were available for analysis. For each correct trial, the direction of movement, its amplitude (Euclidean distance from beginning to end), and the spike discharge rate (from the onset of the target to the end of the movement) were used to calculate directional statistics (Mardia 1972) for the directions of the movements performed, to analyze directional tuning of cell activity and to calculate the NPV.

Directional tuning

Estimation using directional statistics

The preferred direction of a cell ("mean direction") was determined as follows (Mardia 1972, p. 25).

$$X = \sum_{i=1}^{N} f_\theta \cos\theta \tag{1}$$

$$Y = \sum_{i=1}^{N} f_\theta \sin\theta \tag{2}$$

$$Q = \sum_{i=1}^{N} f_\theta \tag{3}$$

$$\bar{X} = \frac{X}{Q} \tag{4}$$

$$\bar{Y} = \frac{Y}{Q} \tag{5}$$

$$x_0 = \tan^{-1}\left(\frac{Y}{X}\right) \tag{6}$$

$$R = \left(X^2 + Y^2\right)^{1/2} \tag{7}$$

$$\bar{R} = \left(\bar{X}^2 + \bar{Y}^2\right)^{1/2} \tag{8}$$

$$s_0 = \left(-2\ln\bar{R}\right)^{1/2} \tag{9}$$

where θ is the direction of the movement, N is the number of movements (trials) that the monkey did for the cell analyzed, f_θ is the discharge rate of the cell for movement θ (from the onset of the target stimulus to the end of movement), $\bar{x}_0$ is the mean direction (i.e., preferred direction) of the cell, R is the resultant, $\bar{R}$ is the mean resultant, and s_0 is the circular standard deviation (in radians, converted to degrees). Expressed as an x–y vector, the preferred direction is $\vec{C}$. Since the measurements above describe basically a tuning curve in the unit circle, we took as a measure of tuning width one-half of the circular standard deviation:

$$s_0' = \frac{s_0}{2} \tag{10}$$

The measure s_0' corresponds roughly to the half-width (at mid-height) of the tuning curve.

Estimation using regression analysis

In this analysis, we evaluated directional tuning by fitting a model from the von Mises distribution (Mardia 1972), appropriate for circular data, in order to obtain an estimate of goodness of fit and a statistical significance level. The model was as follows:

$$d = a\mathrm{e}^{\kappa\cos(\theta-\theta_0)} \tag{11}$$

where d is the discharge rate, a and κ are constants, θ is the direction of the movement, and θ_0 is the cell's preferred direction. By taking the logs and adding the constant 1/2 to d to avoid occasional division by zero and stabilize the variance (Cox and Lewis 1966), we have:

$$d' = \ln\left(d + \frac{1}{2}\right) = \ln(a) + \kappa\cos(\theta - \theta_0) \tag{12}$$

Equation 12 is equivalent to

$$d' = \ln(a) + b_1\sin(\theta) + b_2\cos(\theta) \tag{13}$$

The preferred direction is given by

$$\hat{\theta}_0 = \tan^{-1}\left(\frac{b_1}{b_2}\right) \tag{14}$$

and

$$\hat{\kappa} = \left(b_1^2 + b_2^2\right)^{1/2} \tag{15}$$

The half-width (at mid-height) H of the tuning curve is a power function of $\hat{\kappa}$, as shown in Fig. 2 in Mahan and Georgopoulos (2013). In the present study, it was estimated

empirically by fitting the tuning function (Eq. 13) and calculating its half-width (at mid-height) by an iterative procedure at 1° resolution.

The tuning function analysis above provided a probability value ($P < 0.05$) by which to assess the statistical significance of the tuning model and the percent of variance explained, R^2. Of the total 899 cells, 754 were directionally tuned and were used to calculate NPV (see below).

Movement data

For each set of movements for which an NPV was calculated (see below), we also computed summary statistics for the movement set. Specifically, we computed (1) the average amplitude of the movement, $\bar{m}$, (2) its mean direction θ_m and circular standard deviation m_0 (using directional statistics), and (3) the length of the arc E subtended by m_0 at length $\bar{m}$. Then, we calculated the index of difficulty, I_d (Fitts 1954) according to the revised formula (MacKenzie 1992):

$$I_\mathrm{d} = \log_2\left(1 + \frac{\bar{m}}{E}\right) \tag{16}$$

NPV calculation

NPVs were calculated using weighted vectorial contributions from the 754 directional tuned cells above. Of those cells, 712 (in 6 monkeys) were studied using eight targets in radial directions from the center, every 45°, starting at 3 o'clock. For the remaining 42 cells (in 2 monkeys), 20 targets were placed equidistantly on the circle (every 18°) with a random start location. Those targets were distributed randomly around the fixed eight targets directions above. Let Θ_j be the center of those eight fixed directions ($j = 0, 45, 90, 135, 180, 225, 270, 315°$), starting from 3 o'clock (0°) counterclockwise. We computed NPVs and associated statistics for movement sets with movement directions lying within the sector $S_j = \Theta_j \pm 22.5°$ and for different binned conditions (cell directional spread, overall cell activity, and resting activity—see below).

The NPV, $\vec{\boldsymbol{P}}$ (in x–y coordinates in the unit circle), for a particular movement sector S_j was calculated by summing weighted contributions along the cells' preferred directions:

$$\vec{\boldsymbol{P}}(S_j) = \sum_{i=1}^{M} w_{i\theta}\vec{\boldsymbol{C}}_i \tag{17}$$

where $w_{i\theta}$ is the observed discharge rate of the ith cell for movement θ lying within sector S_j, $\vec{\boldsymbol{C}}_i$ is the cell's preferred direction (in x–y coordinates in the unit circle), and M is the number of trials (movements) in S_j. To simplify notation, we use $\vec{\boldsymbol{P}}$ to mean $\vec{\boldsymbol{P}}(S_j)$ and omit the range (1 to M) in the summing operator $\sum$.

The following quantities were calculated as intermediate steps. Let θ_0^i be the preferred direction of the ith cell in polar coordinates (corresponding to $\vec{\boldsymbol{C}}_i$ in x–y coordinates). Then

$$X_{\vec{\boldsymbol{P}}} = \sum w_{i\theta}\cos\theta_0^i \tag{18}$$

$$Y_{\vec{\boldsymbol{P}}} = \sum w_{i\theta}\sin\theta_0^i \tag{19}$$

$$T = \sum w_{i\theta} \tag{20}$$

$$\bar{X}_{\vec{\boldsymbol{P}}} = \frac{X_{\vec{\boldsymbol{P}}}}{T} \tag{21}$$

$$\bar{Y}_{\vec{\boldsymbol{P}}} = \frac{Y_{\vec{\boldsymbol{P}}}}{T} \tag{22}$$

$$\pi_0 = \tan^{-1}\left(\frac{Y_{\vec{\boldsymbol{P}}}}{X_{\vec{\boldsymbol{P}}}}\right) \tag{23}$$

$$R_{\vec{\boldsymbol{P}}} = (X_{\vec{\boldsymbol{P}}}^2 + Y_{\vec{\boldsymbol{P}}}^2)^{1/2} \tag{24}$$

$$\bar{R}_{\vec{\boldsymbol{P}}} = \left(\bar{X}_{\vec{\boldsymbol{P}}}^2 + \bar{Y}_{\vec{\boldsymbol{P}}}^2\right)^{1/2} \tag{25}$$

$$\sigma_0 = (-2\ln\bar{R}_{\vec{\boldsymbol{P}}})^{1/2} \tag{26}$$

$$\left|\vec{\boldsymbol{P}}\right| = \frac{1}{M}R_{\vec{\boldsymbol{P}}} \tag{27}$$

where θ is the direction of the movement, M is the number of trials that contributed to the NPV calculation, $w_{i\theta}$ is the discharge rate of the ith cell for movement θ, θ_0^i is the preferred direction of the ith cell, π_0 is the direction of the population vector, $R_{\vec{\boldsymbol{P}}}$ is the resultant, $\bar{R}_{\vec{\boldsymbol{P}}}$ is the mean resultant, σ_0 is the circular standard deviation (in radians) of the population vector, and $|\vec{\boldsymbol{P}}|$ is the average length of the NPV. As a measure of directional precision of the population vector ("variable error"), we took one-half of the circular standard deviation:

$$\sigma_0' = \frac{\sigma_0}{2}. \tag{28}$$

Finally, as a measure of directional accuracy of the population vector with respect to the movement sector for which it was computed ("constant error"), we took the angle φ. (in radians, then transformed to degrees) between π_0 and θ_m:

$$\varphi(S_j) = \cos^{-1}(\sin\pi_0\sin\theta_{\bar{m}} + \cos\pi_0\cos\theta_{\bar{m}}). \tag{29}$$

Other statistical analyses

Standard statistical methods were to perform common analyses, including analysis of variance (ANOVA), linear regression, etc. (Snedecor and Cochran 1989). The circular correlation between preferred directions was calculated as described by Fisher and Lee (1983). The SPSS-IBM statistical package (version 21) and Intel Fortran were used to implement the various statistical analyses.

Results

Of the 899 cells total, 754 (83.9 %) showed a statistically significant regression model (Eq. 11; $P < 0.05$). The distributions of the significance probability values and the fraction of variance explained (R^2) in this group of directionally tuned cells are shown in Figs. 1 and 2, respectively.

Directional spread

A key measure of the present analyses is the directional spread (s'_0). Its distribution for the 754 tuned cells is shown in Fig. 3; the distribution did not differ significantly from a normal distribution (Fig. 4; one-sample Kolmogorov–Smirnov test, $Z = 0.74$, $P = 0.64$). As expected, the directional spread s'_0 of the tuning curve calculated directly was highly correlated with H, the half-width (at mid-height) of the tuning curve estimated indirectly from the regression model of Eq. 11 (Spearman correlation = 0.918, $N = 754$, $P < 0.001$). Since s'_0 is a more direct measure, we used s'_0 in the subsequent analyses. In addition, the preferred

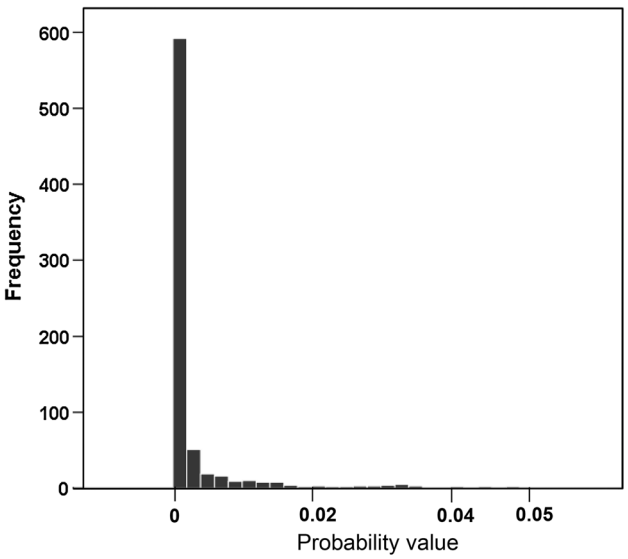

Fig. 1 Frequency distribution of probability values from fitting the regression model of Eq. 13 ($N = 754$ directionally tuned cells)

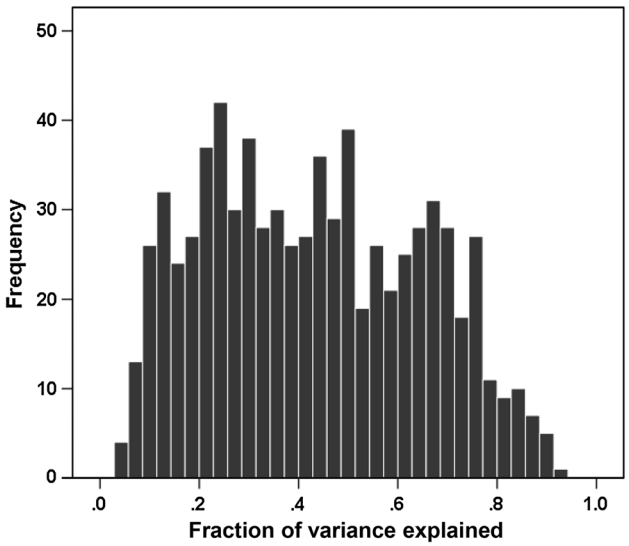

Fig. 2 Frequency distribution of R^2 (fraction of variance explained) from fitting the regression model of Eq. 13 ($N = 754$ tuned cells)

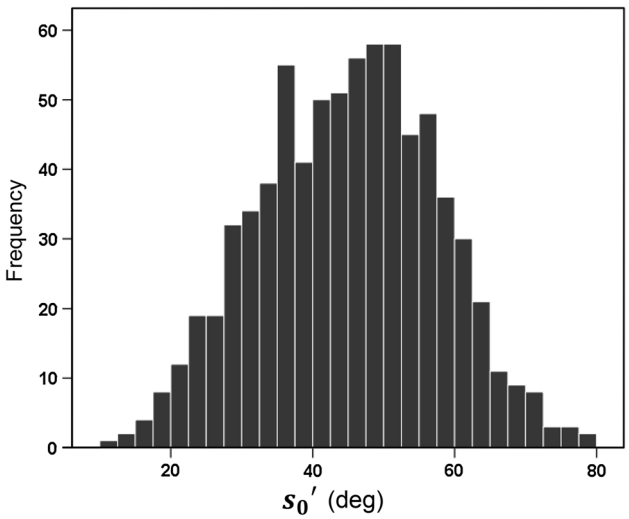

Fig. 3 Frequency distribution of s'_0 (Eq. 10). (see text for details)

directions calculated using the tuning curve ($\hat{\theta}_0$) were highly correlated with those calculated using directional statistics (x_0) (circular correlation coefficient = 0.951, $P < 0.001$).

Directional spread and NPV

To test the hypothesis that NPV properties vary with the directional spread of constituent cells in the population, we binned s'_0 every 10° for the following 7 bins total: ≤20° (15 cells, 161 trials, 11 trials per cell per target movement direction), 21–30° (82, 788, 10), 31–40° (168, 1,420, 8), 41–50° (215, 2,136, 10), 51–60 (187,

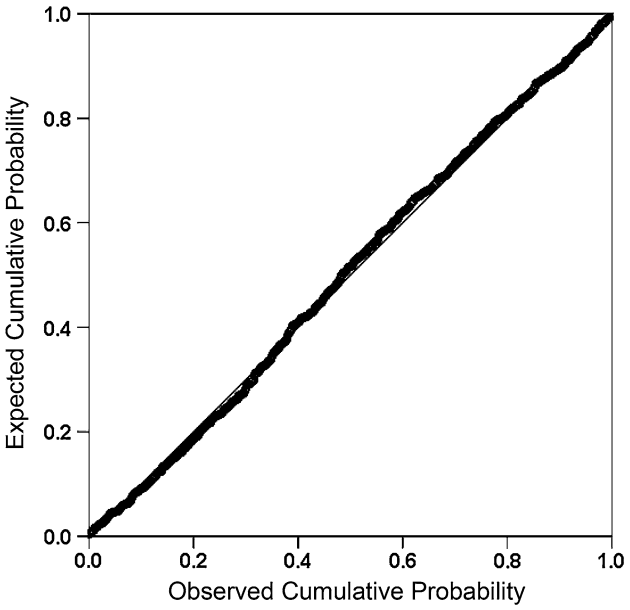

Fig. 4 Probability–probability plot of s_0' (normal distribution)

2,141, 11), 61–70° (71, 771, 11), and >70° (16, 181, 11). The distributions of preferred directions in each bin (Fig. 5) did not differ significantly from a uniform distribution (Rayleigh test, Mardia 1972; $P > 0.05$ for each bin). We then calculated the NPV for each bin and target direction. Figure 6 shows that the NPV variable error, σ_0' increased with tuning directional spread. For the whole data set, a quadratic fit was the best fit (Fig. 7; $P < 0.001$, $r^2 = 0.721$). This relation could be influenced by the number of cells and/or trials entering the calculations, which varied substantially across the 7 bins of s_0' (see above). In order to control for that factor, we calculated the population vector variable error from 100 random bootstrap samples (with replacement) of equal number of cells ($N = 15$) and an upper limit of trials ($N \leq 130$). The results are shown in Fig. 8. It can be seen that essentially the same relation was observed as in the actual, whole sample (Fig. 6).

Similarly, the NPV constant error, φ, increased with directional tuning spread (Figs. 9, 10); for the whole data set, an exponential fit was the best (Fig. 10; $P < 0.001$, $r^2 = 0.432$). In addition, the NPV constant directional error increased as an exponential function of the NPV variable error (Fig. 11; $P < 0.001$, $r^2 = 0.444$). Finally, the average length of the NPV also increased with tuning directional spread (Fig. 12) in an exponential fashion (Fig. 13; $P < 0.001$; $r^2 = 0.420$).

Cell activity, directional tuning, and NPV

The results above document the dependence of NPV on directional tuning spread. If, as we hypothesized (Mahan and Georgopoulos 2013), the directional tuning spread depends, in turn, on the strength of the inhibitory drive, one would expect that there should be an association between the overall cell activity and the sharpness of directional tuning. Indeed, we found a highly significant positive correlation between the sharpness of directional tuning and the

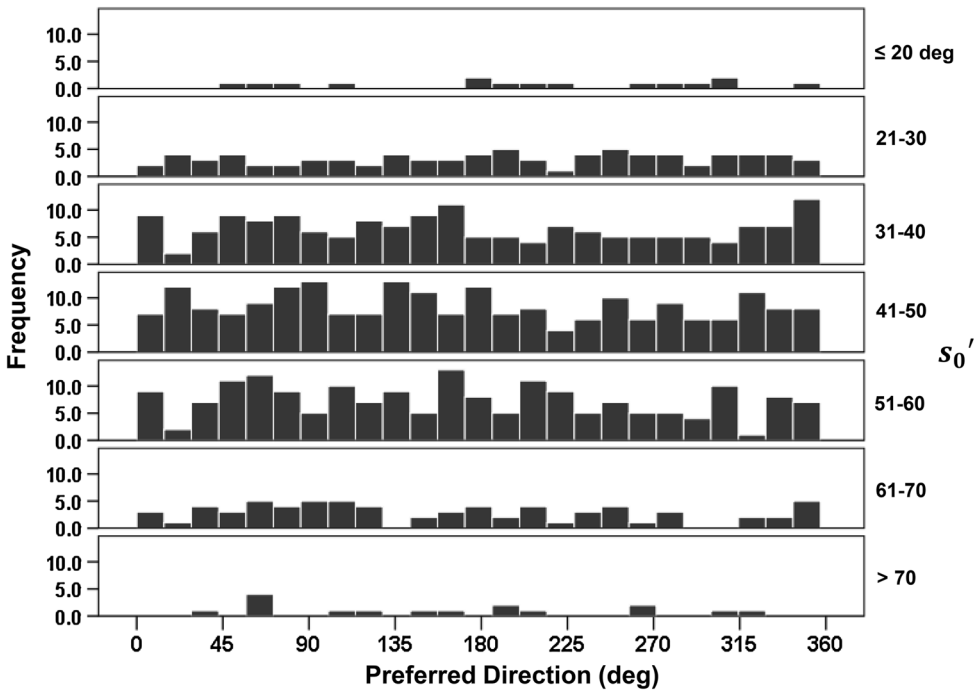

Fig. 5 Frequency distributions of preferred directions of directionally tuned cells with different (binned) s_0' (see text for details)

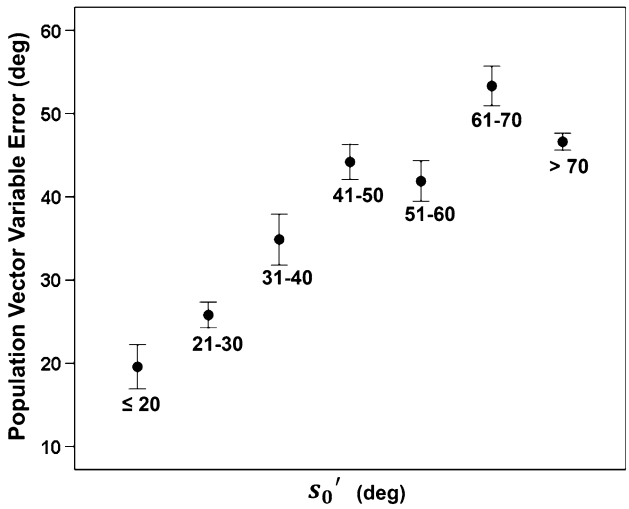

Fig. 6 The mean ± SEM of the NPV variable error, σ_0', is plotted against s_0' ($N = 8$ direction sectors S, per point; see text for details)

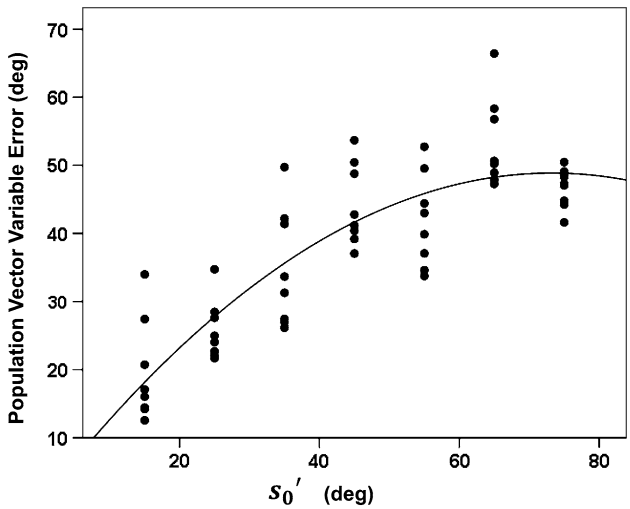

Fig. 7 Scatter plot of σ_0' against s_0'. *Each point* refers to the 8 direction sectors S (see text for details)

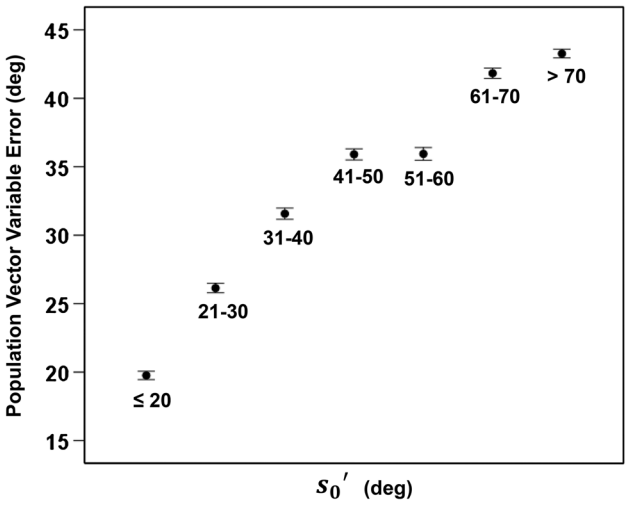

Fig. 8 Results of bootstrap analysis. The mean ± SEM of the NPV variable error calculated from up to 130 trials from 15 cells (with replacement) per s_0' bin is plotted against s_0' ($N = 100$ bootstraps per bin; see text for details)

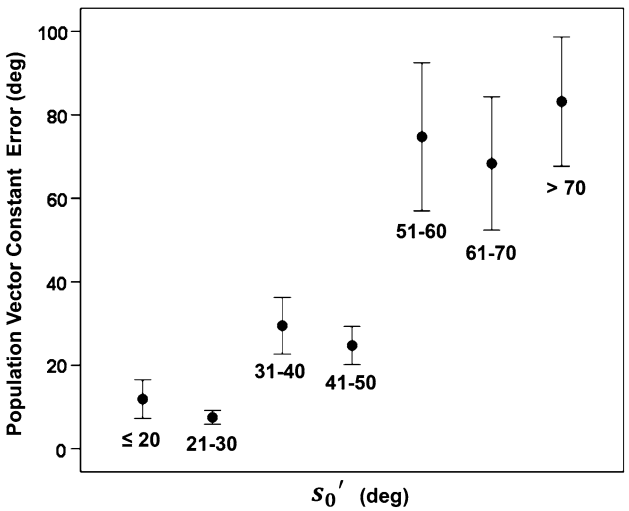

Fig. 9 The mean ± SEM of the NPV constant error, φ, is plotted against s_0' ($N = 8$ direction sectors S; see text for details)

mean firing rate (Fig. 14; $P < 0.001$; $r^2 = 0.238$; $N = 899$ cells). The regression equation was a semi-logarithmic fit:

$$s_0' = 35.06 + 6.097 \ln \bar{D}. \quad (30)$$

where $\bar{D}$ is the overall mean discharge rate of the cell (across all movements). Equation 30 indicates that directional spread increases as a linear function of the logarithm of mean discharge rate. Since deviations from the mean discharge rate vary with tuning parameters (Eq. 12), we performed a separate regression analysis by adding the intercept and coefficient κ as additional independent variables. In this analysis, $\ln \bar{D}$ was again statistically significant ($P < 0.001$) with a positive coefficient; these results document the independent and robust effect of the mean discharge rate on s_0'.

Next, we investigated the relation between the accuracy (i.e., constant error, φ) of the NPV (calculated from all 899 cells) and mean cell discharge rate. For that purpose, we binned $\ln \bar{D}$ in 6 equal intervals and calculated the NPV from cells whose mean discharge rate fell within each interval. The fitted curve was quadratic (Fig. 15; $P < 0.001$, $r^2 = 0.454$, $N = 6$ intervals × 8 movement directions = 48). It can be seen in Fig. 15 that NPV accuracy was smallest for cells with discharge rate roughly from ~1 to ~8 imp/s (Fig. 15, dotted rectangle), whereas

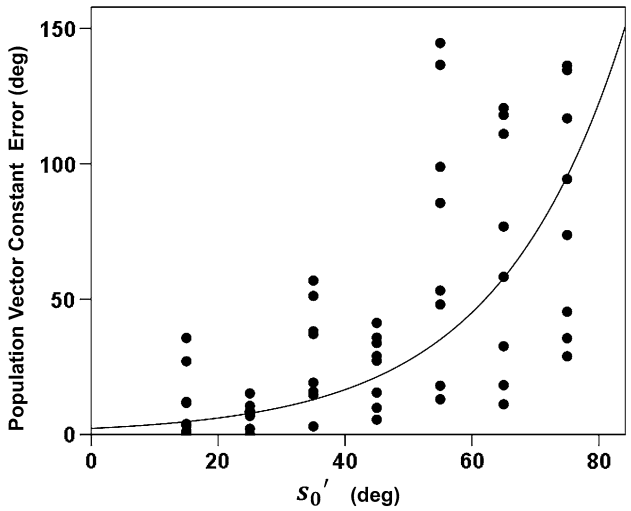

Fig. 10 Scatter plot of φ against s_0'. *Each point* refers to the 8 direction sectors S (See text for details)

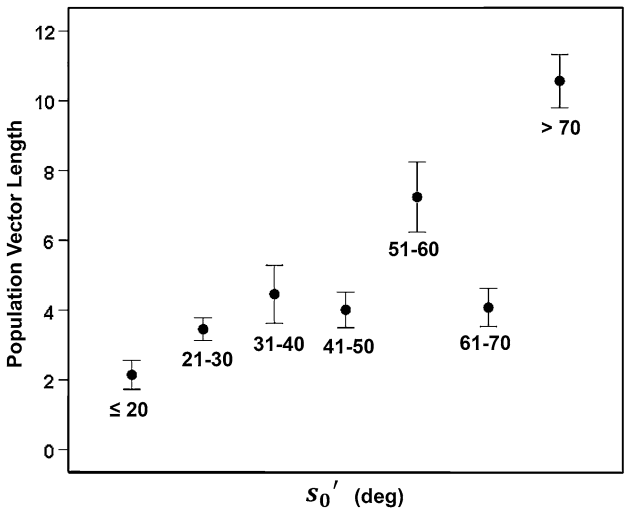

Fig. 12 The mean ± SEM of the NPV length is plotted against s_0' ($N = 8$ direction sectors S; see text for details)

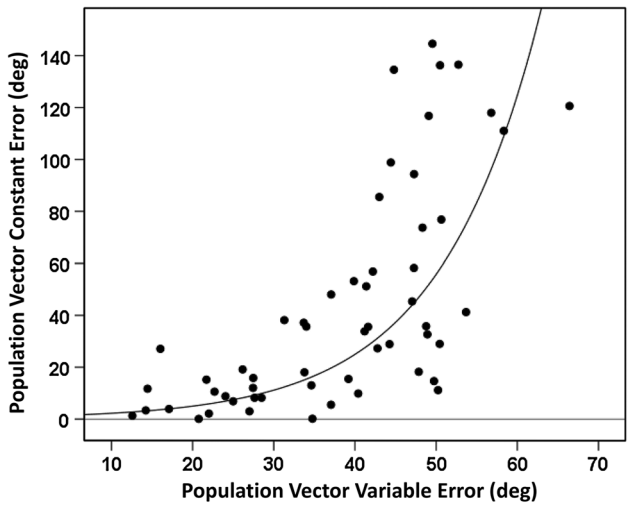

Fig. 11 Scatter plot of φ against π_0'. *Each point* refers to the 8 direction sectors S (see text for details)

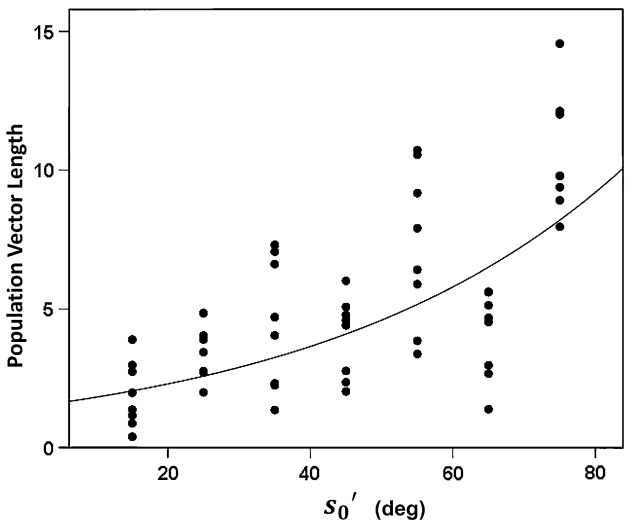

Fig. 13 Scatter plot of NPV length is plotted against s_0'. *Each point* refers to the 8 direction sectors S (see text for details)

NPV accuracy decreased for lower and higher rates. NPV precision (variable error, σ_0') was significantly and positively correlated with NPV accuracy ($r = 0.569$, $P < 0.001$, $N = 48$).

In all analyses above, the NPV was calculated using Eqs. 18–20, where the weight $w_{i\theta}$ for vectorial cell contributions was the discharge rate of the ith cell for movement θ. Now, in previous studies, NPV has been calculated using weights obtained by subtracting the overall mean cell activity $\bar{D}$ from the cell activity D_θ observed for a specific movement in direction θ (Georgopoulos et al. 1983), or by further dividing that difference by the overall mean $\bar{D}$:

$$w'_{i\theta} = \left(\frac{D_\theta - \bar{D}}{\bar{D}}\right). \tag{31}$$

In fact, this weighting gave the most accurate NPV results (Georgopoulos et al. 1988, Table 2, weight #6 in Appendix 2). Indeed, using the weight of Eq. 31 improved the NPV accuracy very much in the present study, such that very accurate NPVs were obtained for a range of mean cell activity from ~1 to ~33 imp/s (Fig. 16, dotted rectangle). The question is why such improvement? The answer seems to be that the weight of Eq. 31 greatly reduced the directional spread in the directional tuning function, thus resulting in greater NPV

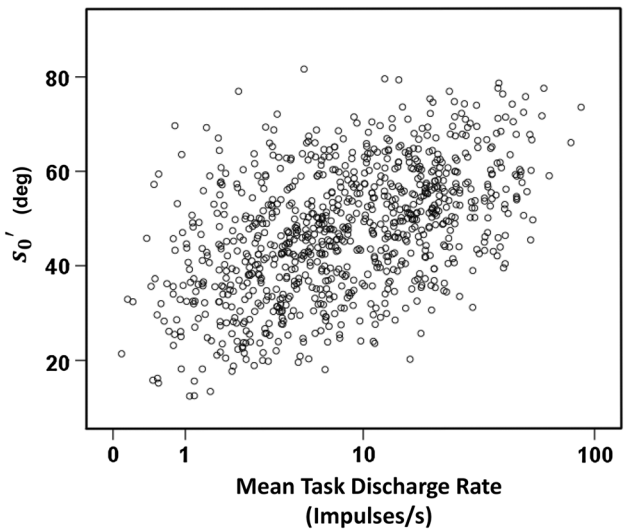

Fig. 14 Scatter plot of s_0' against the mean discharge rate across all movements ($N = 899$ cells) (see text for details)

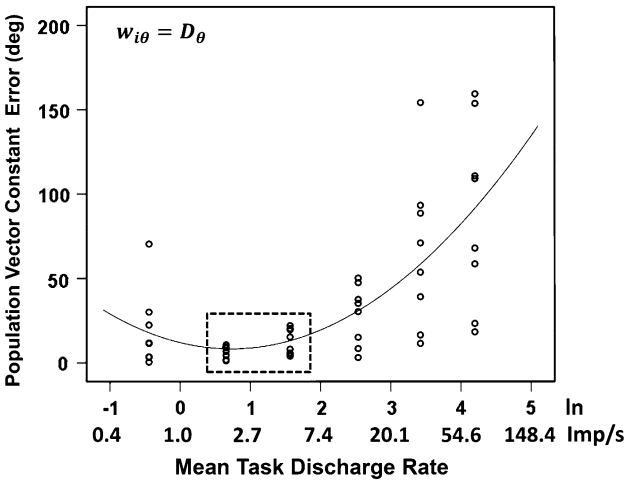

Fig. 15 The NPV constant error, φ, is plotted against binned mean discharge rate in a log scale, when the NPV was calculated using the weight of Eq. 17 (*inset* on *left top*). The *dotted rectangle* demarcates cell rates resulting in highest NPV accuracy (i.e., minimum constant error). *Each point* refers to the 8 direction sectors *S*

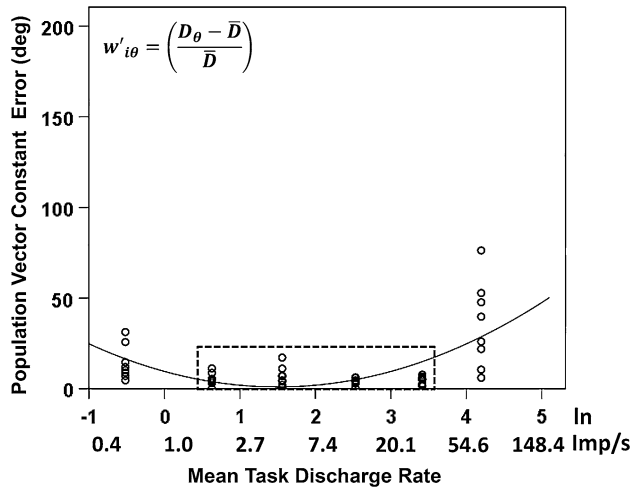

Fig. 16 The NPV constant error, φ, is plotted against binned mean discharge rate in a log scale, when the NPV was calculated using the weight of Eq. 31 (*inset* on *left top*). The *dotted rectangle* demarcates cell rates resulting in highest NPV accuracy (i.e., minimum constant error). *Each point* refers to the 8 direction sectors *S*. The *inset* on *left top* indicates the scalar weight used in calculating the population vector

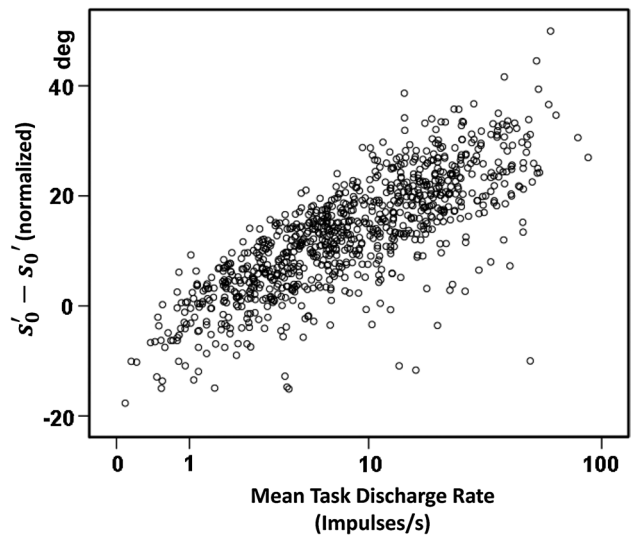

Fig. 17 Scatter plot of $s_0' - s_0'$ (*normalized*) against the mean discharge rate across all movements ($N = 899$ cells) (see text for details)

accuracy, according to the considerations above. In fact, the magnitude of decrease in directional spread was a linear function of $\ln \bar{D}$ (Fig. 17; $P < 0.001$; $r^2 = 0.630$; $N = 899$ cells). The regression equation was as follows:

$$s_0' - s_0' \text{ (normalized)} = -2.59 + 7.76 \ln \bar{D}. \quad (32)$$

Resting cell activity, directional tuning, and NPV

The analyses above dealt with cell discharge during the reaching task and its relations with directional tuning and NPV attributes. In this section, we report on the relations between cell discharge during a resting state, preceding the onset of stimulus ("control period" in Georgopoulos et al. 1982) and the aforementioned variables. The intensity of cell discharge during the control period reflects the net quasi steady-state effect of excitatory/inhibitory inputs on the cell and, hence, can be considered as a stable functional property of the cell, in the absence of phasic inputs. More specifically, we tested the hypothesis that this activity

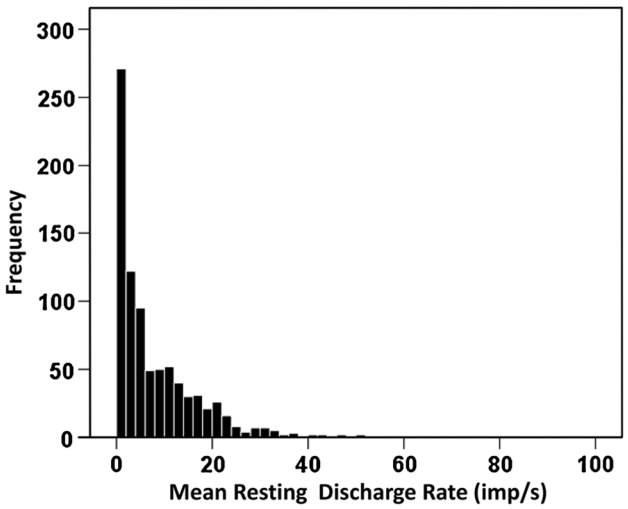

Fig. 18 Frequency histogram of mean resting discharge rates ($N = 849$ cells; see text for details)

would be a good predictor of (a) the overall mean activity during the task, (b) the sharpness of directional tuning, (c) the NPV variable error, and (d) the NPV constant error. If these relations were to prove significant, resting cell activity would acquire a special importance for the neural mechanisms involved in planning a reaching movement with desired directional attributes, since resting activity precedes movement initiation, and therefore, a movement of desired accuracy and precision could be planned by selecting cells based on their resting-state activity.

Eight hundred and forty-nine cells were available for this analysis (control period activity was not recorded for 50 cells). The frequency distribution of the mean resting-state discharge rates is shown in Fig. 18; the best fit was a gamma distribution (Fig. 19). (It should be noted that during the control period from which the "resting" discharge rate was obtained, the monkeys were holding the 2-D manipulandum against a constant gravitational load, such that the activation state of the motor system was very similar across trials and monkeys.) The frequency distribution of the mean task-related discharge rates is shown in Fig. 20; the best fit was a lognormal fit (plots not shown). During the task, 665/849 (78.3 %) cells showed an increase, whereas 184/849 (21.7 %) showed a decrease in activity from the resting state, with similar distributions of the changes (Fig. 21).

The task and resting discharge rates were highly correlated in a log–log scale (Fig. 22; $r = 0.733, P < 0.001$, $N = 841$ cells with resting-state activity greater than zero). This means that the resting-state activity is a good predictor of the ensuing task-related activity, including the associations of the latter with directional tuning and NPV properties. Indeed, the directional tuning spread s'_0 increased with higher resting discharge rates in a log scale (Fig. 23, $r = 0.515, P < 0.001$, $N = 841$ cells with resting-state activity greater than zero). With respect to NPV,

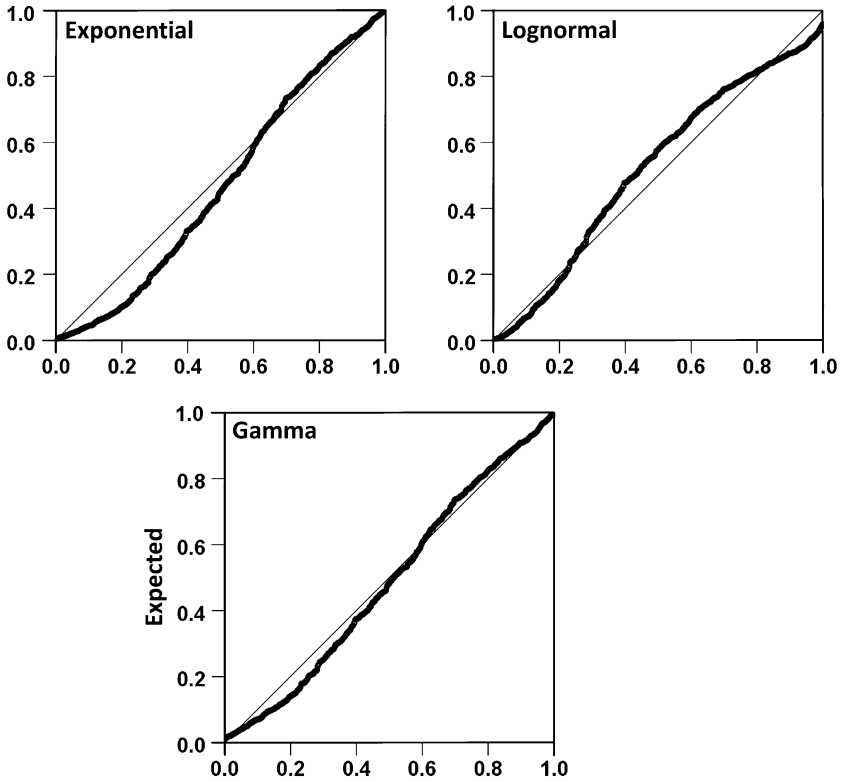

Fig. 19 Cumulative probability–probability plots of mean resting-state discharge rates for three different distribution models, as labeled in the plots. The best fit was a gamma distribution (parameters: shape = 0.818 and scale = 0.103) ($N = 841$ cells with resting activity greater than zero, a condition needed to evaluate the lognormal fit)

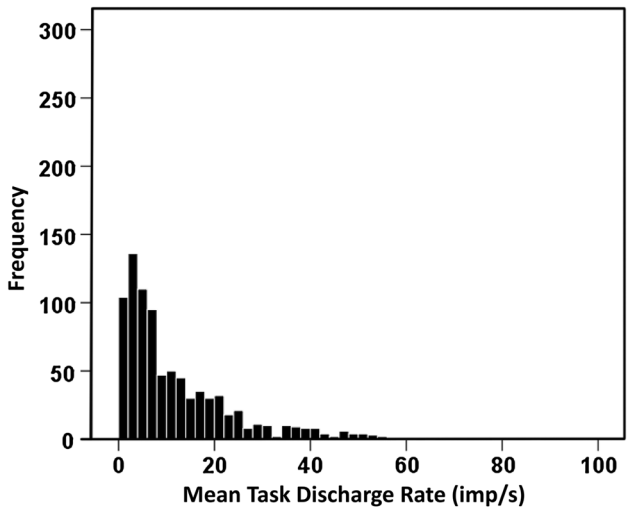

Fig. 20 Frequency histogram of mean task-related discharge rates ($N = 849$ cells; see text for details)

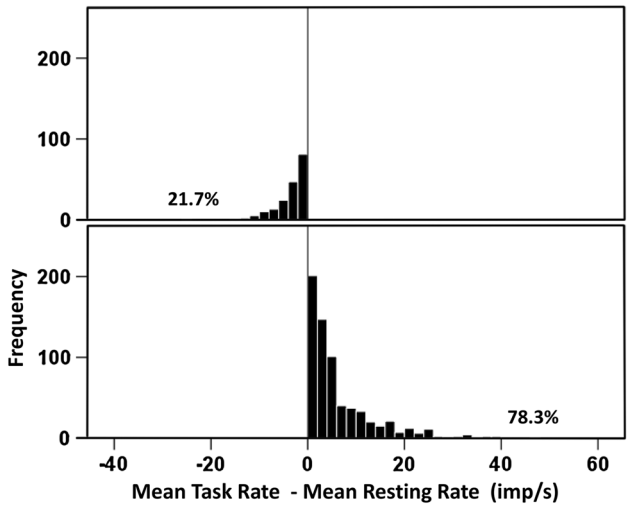

Fig. 21 Frequency distribution of changes in activity between task and resting states ($N = 849$ cells)

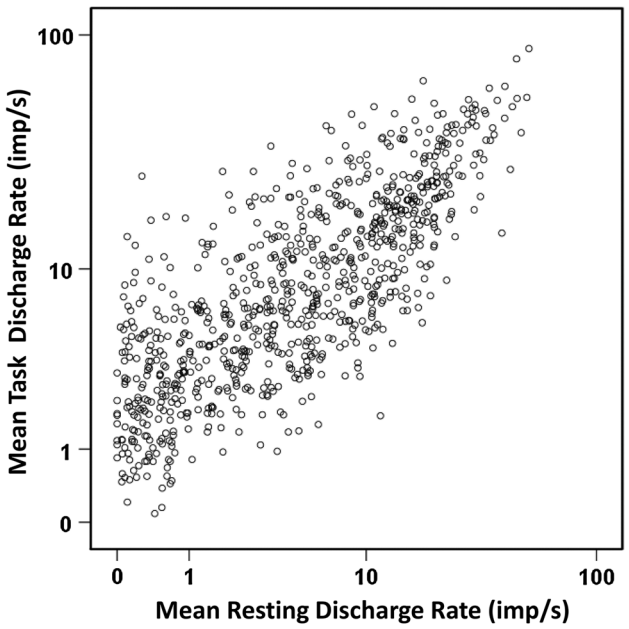

Fig. 22 Scatter plot of mean task-related discharge rate against mean resting-state discharge rate ($N = 849$ cells)

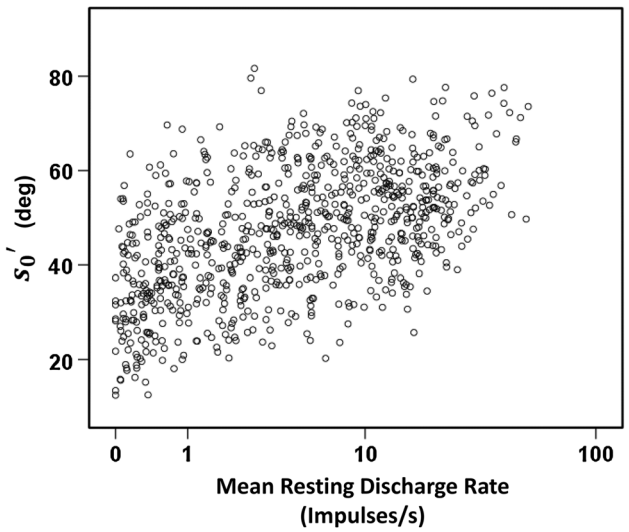

Fig. 23 Scatter plot of s_0' against the mean resting discharge rate across all movements ($N = 849$ cells)

its variable error increased with increasing resting rates ($r = 0.696, P < 0.001$, $N = 48$; data not shown). Similarly, the NPV constant error also increased with increasing log-transformed resting rate (Fig. 24) in a quadratic fit ($r^2 = 0.341, P < 0.001, N = 48$).

NPV and movement attributes

Finally, we analyzed the relations between NPV and movement attributes. We found the following. First, the variable error of the NPV, σ_0', was positively and significantly correlated with that of the movement, m_0 (Fig. 25; $r = 0.418$, $P = 0.003$, $N = 48$). Second, the length of the NPV, $|\vec{P}|$, was positively and significantly correlated with movement amplitude, $\bar{m}$ ($r = 0.619$, $P < 0.001$, $N = 48$). And third, the inverse of the NPV length was positively and significantly correlated with I_d ($r = 0.792$, $P < 0.001$, $N = 48$). Since the length of NPV reflects movement speed (Schwartz 1994), its inverse can be regarded as an neural estimate of movement time, thus positing a neural counterpart of Fitts' Law (Fitts 1954).

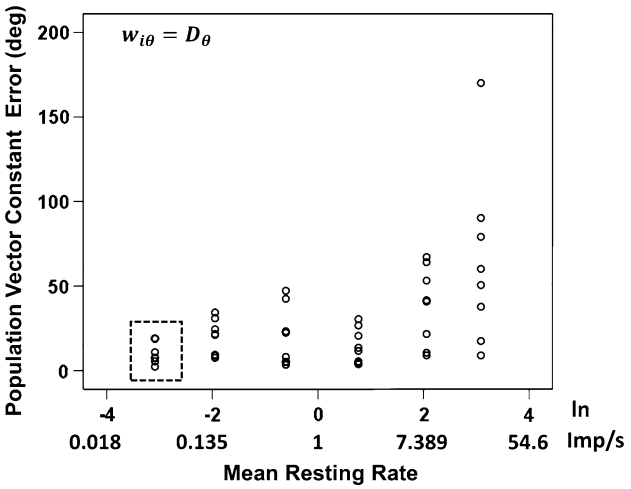

Fig. 24 The NPV constant error, φ, is plotted against binned mean resting discharge rate in a log scale, when the NPV was calculated using the weight of Eq. 17 (*inset* on *left top*). *Each point* refers to the 8 direction sectors *S*

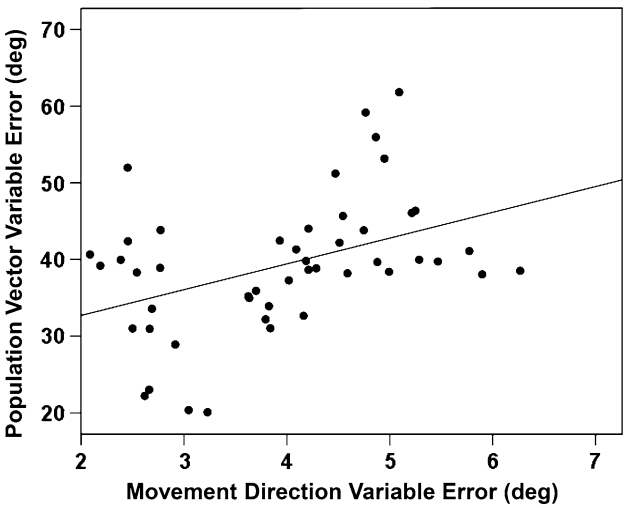

Fig. 25 The NPV variable error, π_0', is plotted against the movement direction variable error mean discharge rate across all movements ($N = 899$ cells) (see text for details)

Discussion

In a recent paper (Mahan and Georgopoulos 2013), we proposed, based on theoretical considerations, that the spread in the cellular directional tuning function could be the mechanism by which the directional precision and accuracy of the NPV, and of the subsequent movement, could be controlled. These considerations were inspired by the known facts concerning the role of Renshaw cells in the spinal cord in sharpening the excitatory field in motoneuronal pools depending on the goal of the motor output, namely whether the intended force production is precise and accurate, or just strong (Hultborn and Pierrot-Deseilligny 1979). It has been shown that the activity of Renshaw cells is controlled centrally, such that Renshaw cells can serve as variable gain regulators (Hultborn et al. 1979): An increase in their activity would result in spatial focusing of spinal motor excitation, leading to a precise motor output, whereas a decrease in their activity would result in a wider excitatory drive, leading to an overall strong but less precise motor output. We hypothesized that a similar role could be served by inhibitory interneurons in various brain motor areas involved in the specification of the motor command (Mahan and Georgopoulos 2013). This hypothesis was based on two ideas, namely (a) that the directional tuning curve is the result of local tangential interactions (Georgopoulos and Stefanis 2007, 2010) and (b) that inhibition plays a key role in shaping directional tuning (Georgopoulos and Stefanis 2007; Merchant et al. 2008).

Apart from the qualitative role of inhibition in implementing directional tuning, we proposed, more specifically, that a graded inhibition could serve to control the directional spread of cellular tuning (Mahan and Georgopoulos 2013). Now, for this to have a meaningful effect, it should affect, somehow, the motor command. Since the NPV is the neural representation of the motor command, we hypothesized that the directional spread of cellular tuning would affect attributes of the NPV. Specifically, we proposed the hypothesis that narrow directional spread (effected, e.g., by increased inhibition) would result in a precise and accurate but short NPV, whereas a broad directional spread would result in less precise and relatively inaccurate but longer NPV (Mahan and Georgopoulos 2013). We adduced evidence for this hypothesis by modeling the cellular directional tuning and calculating NPVs from populations of cells with different directional spread. Our modeling results showed that the directional precision of the NPV decreased systematically as the tuning directional spread increased (Mahan and Georgopoulos 2013). In the present study, we used data from neurophysiological recordings in the motor cortex of monkeys to test the hypothesis above in a realistic setting. Indeed, the present findings confirmed the hypothesized dependence of attributes of the NPV (accuracy, precision, and length) on the directional spread of tuning of constituent cells. In addition, we documented the dependence of directional tuning spread on the overall cell discharge rate, which ties the strength of inhibitory drive to the sharpness of directional tuning.

Directional tuning

Directional motor tuning was first described for cells in the motor cortex (Georgopoulos et al. 1982). A cosine function was a good fit for 2-D (Georgopoulos et al. 1982) and 3-D

movements (Schwartz et al. 1988). The cosine function has a fixed half-mid-width, namely at 45°. Although the cosine fit may capture well the directional tuning, it does not allow for variation in the tuning width (Amirikian and Georgopoulos 2000). In addition, the independent variable in fitting a directional tuning curve is the direction of movement, which varies as a von Mises distribution in the unit circle (Mardia 1972), and the directional tuning curve is an exponential function (see Eq. 11 above). Both the cosine and von Mises functions are unimodal, with the peak at the preferred direction. The major difference between the two functions lies in the fact that the cosine function is a linear function of the cosine of the angle between preferred direction and movement direction, whereas the von Mises fit is an exponential function of that quantity. The latter allows for a continuously varying directional tuning width (possible range 0–90° half-mid-width), depending on the value of the concentration parameter κ. (Eq. 11). In fact, a detailed examination of the directional tuning function using the von Mises distribution revealed a substantial variation in tuning width, with an median half-width (at mid-height) of 28° (Amirikian and Georgopoulos 2000). Based on these considerations, we used the von Mises fit to identify 754/899 (84 %) cells with statistically significant directional tuning (Eq. 11).

Directional spread, NPV, and movement

Directional spread can be measured in different ways. For example, the concentration parameter κ. can be estimated from the tuning function (Eq. 11) but this involves fitting a function. A more direct way to measure directional spread is by calculating the length of the mean resultant $\bar{R}$ from the distribution of movement directions weighted by the cell's discharge rate (Eq. 8) (The parameter $\hat{\kappa}$ can be derived from $\bar{R}$ using maximum likelihood; see Mardia 1972, p. 298). Now, $\bar{R}$ can be transformed to an angle (circular standard deviation, s_0, Eq. 9), and half of that angle (s_0', Eq. 10) is similar to the tuning curve half-width (at mid-height). Hence, we used s_0' in our analysis, as a direct measure of directional spread. As predicted by our modeling studies (Mahan and Georgopoulos 2013), both NPV accuracy (constant error; Figs. 8, 9) and precision (variable error; Figs. 6, 7) increased as directional tuning spread decreased.

Given the above considerations, we investigated the dependence of NPV accuracy and precision directly on the mean task-related cell activity (and resting-state activity), bypassing the intermediate effect on directional spread. We found an interesting quadratic relation, as shown in Figs. 13 and 24. It can be seen that there is an "optimal" region of mean cell activity, roughly between 1 and 8 imp/s in task activity (Fig. 13) (and <0.135 imp/s for resting activity; Fig. 24), where the NPV accuracy is at maximum (i.e., NPV constant error is at minimum; dotted rectangles in Fig. 13 and 24). This range widened substantially (Fig. 14) when a normalized weight, with respect to the overall mean cell activity, was used (Eq. 31), as is commonly the case for calculating the NPV in previous studies. Remarkably, this normalization effected a substantial reduction in directional spread, proportional to the mean discharge rate (Fig. 15), which could account for enhanced accuracy of NPV.

Finally, the calculation of NPV for different combinations of movement directions and cell activity provided adequate variation to assess the relations between attributes of movement and NPV. We found that directional precision and length of NPV were significantly associated with the directional precision of movement (in a set of movements) and average movement amplitude, respectively. In addition, an estimate of neural movement time (calculated as the inverse of NPV length) followed Fitts' Law, being significantly associated with the index of movement difficulty I_d (Eq. 16).

The role of inhibition

These findings bring back the focus on the possible role of inhibition in shaping the motor command. This was the central idea by which we interpreted the results of our modeling studies (Mahan and Georgopoulos 2013), namely that an independent control of the inhibitory drive in a local circuit would modulate the directional spread and thus control the accuracy and precision of the NPV. However, the mechanisms for implementing this idea would be fairly complicated because, somehow, a scalar (such as the amount of inhibitory drive) would have to be translated into a continuous variation/reshaping of the tuning curve. Now, here we discovered a simple link that could mediate the above mechanism via a hard-wired local wiring scheme. Specifically, we found that directional spread was a linear function of the logarithm of the mean cell discharge rate (Fig. 12); there is no a priori reason why such a relation should hold. This relation means that a nonspecific, general-purpose excitatory–inhibitory balance is translated into a fairly sophisticated tuning function with varying directional spread. It is reasonable to assume that the shape of the tuning curve is determined by hardwired local connectivity and that inhibition plays a prominent role in determining the net neuronal activity. Inputs to cortical inhibitory interneurons have typically included that from recurrent pyramidal cell collaterals and external inputs (e.g., from the thalamus) which impinge on various kinds of cells in the column. We postulate the presence of a dedicated, specific, and private input to inhibitory interneurons; to our knowledge, this issue remains to be investigated.

Relation to orientation tuning in the visual cortex (V1)

The analysis above dealt exclusively with reaching movements and motor cortical cells. However, the role of inhibition in shaping tuning in the visual cortex has been actively investigated since the early observations on intracortical inhibition by Benevento et al. (1972). Although this subject has been hotly contested over the years (see Ferster and Miller 2000 for a review), there is currently general agreement that inhibition plays a major role in sharpening the orientation selectivity of V1 cells, as evidenced by theoretical studies (Troyer et al. 1998; Kang et al. 2003) as well as neurophysiological and pharmacological studies in various animal species (Sillito 1975, 1979; Li et al. 2008, 2012a, b; see Shapley et al. 2003 for a review). More specifically, general, nonspecific, "untuned" inhibition is thought to be the local cortical network mechanism by which weak excitation around a focused excitatory drive at the preferred orientation is eliminated, thus resulting in a sharpened orientation selective tuning curve in primate V1 (Xing et al. 2011). This hypothesis has been thoroughly investigated, and the results quantitatively documented (Shapley et al. 2003; Xing et al. 2011). In a way, this idea is very similar to the role of Renshaw inhibition in the spinal cord in sharpening the locus of motoneuron excitation by eliminating weak excitatory fringe (Hultborn et al. 1979) and the effect of recurrent inhibition in the motor cortex in spatial sharpening of the focus of excitation (Stefanis and Jasper 1964; Stefanis 1969; Georgopoulos and Stefanis 2007, 2010).

The population vector, motor and visual, as the means for implementing desired behavioral performance

Altogether, the results of this study and their interpretation above are in the same vein as those by Shapley and colleagues for V1 (Shapley et al. 2003; Xing et al. 2011) and, combined, underscore the statement that "Finding more about the mechanisms of increased cortical selectivity is important for understanding how the cortex works" (Xing et al. 2011, abstract). Now, the new idea that we proposed in a previous paper (Mahan and Georgopoulos 2013) is that the magnitude of this inhibitory drive can be modulated independently of local cortical circuit interactions for the explicit purpose of achieving a behavioral goal, namely to generate a movement of specified directional precision and accuracy (see Fig. 5 in Mahan and Georgopoulos 2013). The results of the present study cemented the connection between sharpness of cell directional tuning and directional precision and accuracy of the population vector (higher sharpness → higher population vector precision and accuracy), and addressed indirectly the relation between sharpness of directional tuning and degree of net excitation (lower mean discharge rates → higher sharpness). Then, the connection between mean discharge rate and population vector precision and accuracy was established (Figs. 15, 16). Remarkably, this connection was extended and documented with respect to the mean discharge rate during a resting state preceding the movement (Fig. 24). What is lacking is a direct association between inhibition, mean discharge rate (resting or task-related), sharpness of tuning, and behavioral precision/accuracy. Evidence for such a direct association was provided by the results of an optogenetic study in the visual cortex of the mouse (Lee et al. 2012). In that study, optogenetic activation of parvalbumin-positive (PV^+) inhibitory interneurons in the visual cortex (a) lowered mean discharge rate of nearby neurons, (b) sharpened their orientation tuning, and (c) improved perceptual discrimination of orientation gratings. Moreover, using proper control procedures, it was shown that these effects were due to inhibition and not disfacilitation (Lee et al. 2012). These results tie all loose ends together, so to speak, and would be expected to apply as well to motor cortex and other cortical areas.

Visual population vector

Lee et al. (2012) also showed that awake, behaving mice discriminated better two orientation gratings when PV^+ interneurons were activated, and the electrophysiological effects above were also observed in the awake mice. These results point to an orientation population signal whose orientation selectivity is higher (i.e., its variable error is lower) under PV^+ optogenetic stimulation. This population visuocortical orientation signal would be formally equivalent to our motor population vector in that they are both weighted vectorial averages of cell contributions along their preferred orientation (range 0–180°) or movement direction (range 0–360°), for visual or motor cells, respectively. However, although the motor population vector was calculated more than 30 years ago (Georgopoulos et al. 1983), the visual one remains to be computed. We predict that the properties of the visual population vector would vary in a similar fashion to that described in this paper in association with sharpness of orientation tuning and log mean discharge rate, i.e., the overall inhibitory drive. As in the motor system, a direct modulation of this inhibitory drive could be the underlying mechanism for task-dependent visual orientation discrimination.

Possible role of inhibition in cognitive processing

The results of this study, and those of other studies discussed above, clearly point to an important role of inhibition in shaping behavioral outcomes, including movement accuracy and visual perception. Since the NPV has been

instrumental in visualizing time-varying, dynamically evolving cognitive processing, including mental rotation (Georgopoulos et al. 1989; Lurito et al. 1991), memory scanning (Pellizzer et al. 1995), and mental tracing in maze solving (Crowe et al. 2005), and since NPV directional accuracy and precision are directly affected by inhibition, it is reasonable to suppose that the amount of inhibition will affect cognitive processing and performance. This hypothesis is supported by the results of Lee et al. (2012) discussed above, where optogenetic activation of PV^+ inhibitory interneurons in the visual cortex improved perceptual discrimination of orientation gratings. Similarly, an increase in the inhibitory drive in relevant cortical circuits (effected, for example, by appropriate optogenetic stimulation) would result in an improved cognitive performance in mental rotation, memory scanning, maze solving, and other tasks, stemming from a more accurate and precise time-varying NPV. This hypothesis remains to be investigated.

Acknowledgments This work was supported by the American Legion Brain Sciences Chair, University Minnesota.

References

Amirikian B, Georgopoulos AP (2000) Directional tuning profiles of motor cortical cells. Neurosci Res 36:73–79

Benevento LA, Creutzfeldt OD, Kuhnt U (1972) Significance of intracortical inhibition in the visual cortex. Nat New Biol 238:124–126

Cox DR, Lewis PAW (1966) The statistical analysis of series of events. Chapman Hall, London

Crowe DA, Averbeck BB, Chafee MV, Georgopoulos AP (2005) Dynamics of parietal neural activity during spatial cognitive processing. Neuron 47:885–891. doi:10.1016/j.neuron.2005.08.005

Ferster D, Miller KD (2000) Neural mechanisms of orientation selectivity in the visual cortex. Annu Rev Neurosci 23:441–471. doi:10.1146/annurev.neuro.23.1.441

Fisher NI, Lee AJ (1983) A correlation coefficient for circular data. Biometrika 70:327–332

Fitts PM (1954) The information capacity of the human motor system in controlling the amplitude of movement. J Exp Psychol 47:381–391

Georgopoulos AP, Stefanis CN (2007) Local shaping of function in the motor cortex: motor contrast, directional tuning. Brain Res Rev 55:383–389

Georgopoulos AP, Stefanis C (2010) The motor cortical circuit. In: Shepherd G, Grillner S (eds) Brain microcircuits. Oxford, New York, pp 39–45. doi:10.1016/j.brainresrev.2007.05.001

Georgopoulos AP, Kalaska JF, Caminiti R, Massey JT (1982) On the relations between the direction of two-dimensional arm movements and cell discharge in primate motor cortex. J Neurosci 2:1527–1537

Georgopoulos AP, Caminiti R, Kalaska JF, Massey JT (1983) Spatial coding of movement: a hypothesis concerning the coding of movement direction by motor cortical populations. Exp Brain Res Suppl 7:327–336

Georgopoulos AP, Schwartz AB, Kettner RE (1986) Neuronal population coding of movement direction. Science 233:1416–1419

Georgopoulos AP, Kettner RE, Schwartz AB (1988) Primate motor cortex and free arm movements to visual targets in three-dimensional space. II. Coding of the direction of movement by a neuronal population. J Neurosci 8:2928–2937

Georgopoulos AP, Lurito JT, Petrides M, Schwartz AB, Massey JT (1989) Mental rotation of the neuronal population vector. Science 243:234–236

Hultborn H, Pierrot-Deseilligny E (1979) Changes in recurrent inhibition during voluntary soleus contractions in man studied by an H-reflex technique. J Physiol (Lond) 297:229–251

Hultborn H, Lindstrom S, Wigstrom H (1979) On the function of recurrent inhibition in the spinal cord. Exp Brain Res 37:399–403

Kang K, Shelley M, Sompolinsky H (2003) Mexican hats and pinwheels in visual cortex. Proc Natl Acad Sci USA 100:2848–2853. doi:10.1073/pnas.0138051100

Lee SH, Kwan AC, Zhang S, Phoumthipphavong V, Flannery JG, Masmanidis SC, Taniguchi H, Huang ZJ, Zhang F, Boyden ES, Deisseroth K, Dan Y (2012) Activation of specific interneurons improves V1 feature selectivity and visual perception. Nature 488:379–383. doi:10.1038/nature11312

Li G, Yang Y, Liang Z, Xia J, Yang Y, Zhou Y (2008) GABA-mediated inhibition correlates with orientation selectivity in primary visual cortex of cat. Neuroscience 155:914–922. doi:10.1016/j.neuroscience.2008.06.032

Li YT, Ma WP, Pan CJ, Zhang LI, Tao HW (2012a) Broadening of cortical inhibition mediates developmental sharpening of orientation selectivity. J Neurosci 32:3981–3991. doi:10.1523/JNEUROSCI.5514-11.2012

Li YT, Ma WP, Li LY, Ibrahim LA, Wang SZ, Tao HW (2012b) Broadening of inhibitory tuning underlies contrast-dependent sharpening of orientation selectivity in mouse visual cortex. J Neurosci 32:16466–16477. doi:10.1523/JNEUROSCI.3221-12.2012

Lurito JT, Georgakopoulos T, Georgopoulos AP (1991) Cognitive spatial-motor processes. 7. The making of movements at an angle from a stimulus direction: studies of motor cortical activity at the single cell and population levels. Exp Brain Res 87:562–580

MacKenzie SI (1992) Fitts' law as a research and design tool in human–computer interaction. Hum Comput Interact 7:91–139

Mahan MY, Georgopoulos AP (2013) Motor directional tuning across brain areas: directional resonance and the role of inhibition for directional accuracy. Front Neural Circuits 7:92. doi:10.3389/fncir.2013.00092

Mardia KV (1972) Statistics of directional data. Academic Press, New York

Merchant H, Naselaris T, Georgopoulos AP (2008) Dynamic sculpting of directional tuning in the primate motor cortex during three-dimensional reaching. J Neurosci 28:9164–9172. doi:10.1523/JNEUROSCI.1898-08.2008

Pellizzer G, Sargent P, Georgopoulos AP (1995) Motor cortical activity in a context-recall task. Science 269:702–705

Schwartz AB (1994) Direct cortical representation of drawing. Science 265:540–542

Schwartz AB, Kettner RE, Georgopoulos AP (1988) Primate motor cortex and free arm movements to visual targets in three-dimensional space. I. Relations between single cell discharge and direction of movement. J Neurosci 8:2913–2927

Shapley R, Hawken M, Ringach DL (2003) Dynamics of orientation selectivity in the primary visual cortex and the importance of cortical inhibition. Neuron 38:689–699

Sillito AM (1975) The contribution of inhibitory mechanisms to the receptive field properties of neurones in the striate cortex of the cat. J Physiol 250:305–329

Sillito AM (1979) Inhibitory mechanisms influencing complex cell orientation selectivity and their modification at high resting discharge levels. J Physiol 289:33–53

Snedecor GW, Cochran WG (1989) Statistical methods. Iowa State University Press, Ames, IA

Stefanis C (1969) Interneuronal mechanisms in the cortex. In: Brazier MAB (ed) The interneuron. University of California Press, Berkeley, pp 497–526

Stefanis C, Jasper H (1964) Recurrent collateral inhibition in pyramidal tract neurons. J Neurophysiol 27:855–877

Troyer TW, Krukowski AE, Priebe NJ, Miller KD (1998) Contrast-invariant orientation tuning in cat visual cortex: thalamocortical input tuning and correlation-based intracortical connectivity. J Neurosci 18:5908–5927

Xing D, Ringach DL, Hawken MJ, Shapley RM (2011) Untuned suppression makes a major contribution to the enhancement of orientation selectivity in macaque v1. J Neurosci 31:15972–15982. doi :10.1523/JNEUROSCI.2245-11.2011